ELSEVIER

Journal of Biomechanics 33 (2000) 1543–1549

JOURNAL OF BIOMECHANICS

www.elsevier.com/locate/jbiomech

Tensegrity architecture explains linear stiffening and predicts softening of living cells

K.Yu. Volokh*, O. Vilnay, M. Belsky

Faculty of Civil Engineering, Israel Institute of Technology, Technion, Haifa 32000, Israel

Accepted 3 July 2000

Abstract

The problem of theoretical explanation of the experimentally observed linear stiffening of living cells is addressed. This explanation is based on Ingber's assumption that the cell cytoskeleton, which enjoys tensegrity architecture with compressed microtubules that provide tension to the microfilaments, affects the mechanical behavior of the living cell. Moreover, it is shown that the consideration of the extreme flexibility of microtubules and the unilateral response of microfilaments is crucial for the understanding of the living cell overall behavior. Formal nonlinear structural analysis of the cell cytoskeleton under external mechanical loads is performed. For this purpose, a general computer model for tensegrity assemblies with unilateral microfilaments and buckled microtubules is developed and applied to the theoretical analysis of the mechanical response of 2D and 3D examples of tensegrity cells mimicking the behavior of real living cells. Results of the computer simulations explain the experimentally observed cell stiffening. Moreover, the theoretical results predict the possible existence of a transient softening behavior of cells, a phenomenon, which has not been observed in experiments yet.

Keywords: Cell; Cytoskeleton; Tensegrity; Analysis; Stiffening; Softening

1. Introduction

There are some experimental observations of the mechanical behavior of living cells, which are hardly explainable within the framework of simple cell model of a viscous fluid balloon. Harris et al. (1980) found that when affixed to flexible rubber substrata cells contract and become more spherical. This contraction bunches up the underlying rubber. Maniotis et al. (1997) observed that pulling on receptors at the cell surface should produce immediate structural changes deep inside the cell. They demonstrated this directly by binding micropippets to adhesion receptors on the surface of living cells and pulling outward, what caused cytoskeletal filaments and nucleus structures to realign immediately in the direction of the pull.

The experiments mentioned above, however, are readily explained within the framework of Ingber's (1993) assumption that the cytoskeleton, which is enjoying *tensegrity* architecture, plays crucial role in mechanical behavior of living cells. Here tensegrity (tensile + integrity) means that cytoskeletal filaments form cable net pretensioned by compressed struts–microtubules. This structure is the main load bearing part of the cell. Ingber (1998) used a six-strut tensegrity cell shown in Fig. 1 of our paper to model the living cell and demonstrated how this model qualitatively explains the cited experiments. Moreover, this model shows a good correspondence with the linear stiffening response of living cells observed experimentally by Wang et al. (1993) and Wang and Ingber (1994), Thoumine et al. (1995). The *existence* of the stiffening means that the cell response is nonlinear. The latter is inherent in structures enjoying tensegrity architecture (Volokh and Vilnay, 1997a, b; Volokh, 1999).

Recently Coughlin and Stamenovic (1997) underlined that the theoretical tensegrity models of the cytoskeleton should consider the unilateral behavior of cables-filaments and the postbuckling behavior of struts-microtubules because of the extreme flexibility of these biological elements. This is in contrast to the initial Ingber's physical model where struts-microtubules were straight and stiff.

* Corresponding author. Tel.: +972-4-8292413; fax: +972-4-8323433.

E-mail address: cvolokh@aluf.technion.ac.il (K.Yu. Volokh).

0021-9290/00/$ - see front matter
PII: S0021-9290(00)00157-3

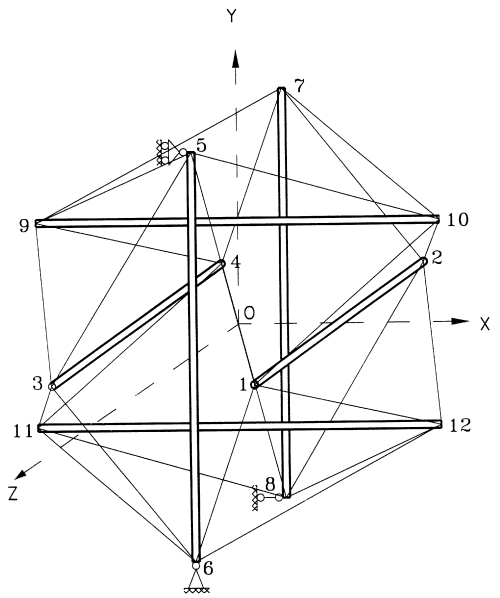

Fig. 1. Space tensegrity cell comprising 6 microtubules and 24 microfilaments.

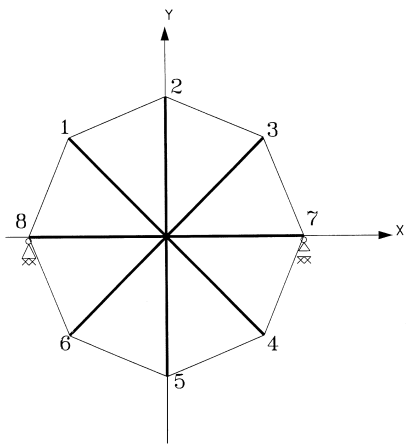

Fig. 2. Plane tensegrity cell comprising 4 microtubules and 8 microfilaments.

In this work it is investigated if the assumption that the cytoskeleton is a tensegrity structure, with unilateral behavior of the microfilaments and buckling and postbuckling of the microtubules, can explain the experimentally observed linear stiffening of the living cells. Particularly, two examples of 4-strut plane and 6-strut space tensegrity models shown in Figs. 1 and 2 are analyzed considering pulling and twisting loads. The elastic properties of the elements of the assemblies are taken from biological data.

2. Methods

Equilibrium equations of tensegrity assemblies may be written in the following form:

$$\mathbf{B}^{\mathrm{T}}\mathbf{p} = \mathbf{q}, \tag{1}$$

where $\mathbf{p}$ is an $m \times 1$ column matrix of axial member forces; $\mathbf{q}$ is an $n \times 1$ matrix of external nodal loads. Matrix $\mathbf{B}$ is obtained from kinematic relationships $\mathbf{e} = \mathbf{e}[\mathbf{u}]$ by using the principle of virtual displacements

$$\mathbf{B} = \frac{\partial \mathbf{e}}{\partial \mathbf{u}}, \tag{2}$$

where $\mathbf{e}$ is a column matrix of axial member strains; and $\mathbf{u}$ is a column matrix of nodal displacements. In order to complete this system of equations it is necessary to add constitutive laws

$$\mathbf{p} = \mathbf{p}[\mathbf{e}]. \tag{3}$$

By substituting Eqs. (2) and (3) into Eq. (1) the displacement form of equilibrium equations is obtained. Newton–Raphson (NR) method solves this system by iterations

$$\overset{i}{\mathbf{K}}\,\overset{i}{\delta\mathbf{u}} = \mathbf{q} - \overset{i}{\mathbf{r}}, \quad \overset{i+1}{\mathbf{u}} = \overset{i}{\mathbf{u}} + \overset{i}{\delta\mathbf{u}}, \quad \overset{0}{\mathbf{u}} = \mathbf{0}, \tag{4}$$

where

$$\overset{i}{\mathbf{r}} = \mathbf{B}^{\mathrm{T}}\mathbf{p}\left[\overset{i}{\mathbf{u}}\right], \quad \overset{i}{\mathbf{K}} = (\mathbf{B}^{\mathrm{T}}\mathbf{C}\mathbf{B} + \mathbf{D})\left[\overset{i}{\mathbf{u}}\right], \tag{5}$$

$$\mathbf{K} = \frac{\partial \mathbf{r}}{\partial \mathbf{u}}, \quad \mathbf{C} = \frac{\partial \mathbf{p}}{\partial \mathbf{e}}, \quad \mathbf{D} = \frac{\partial(\mathbf{B}^{\mathrm{T}}\mathbf{p})}{\partial \mathbf{u}}. \tag{6}$$

Matrix $\mathbf{K}$ is the tangent stiffness matrix; matrix $\mathbf{C}$ is the tangent constitutive modular matrix; and matrix $\mathbf{D}$, computed at $\mathbf{p} = \text{const}$, is the geometric stiffness matrix. In the case where the strain potential ψ exists all calculations are simplified

$$\mathbf{p} = \frac{\partial \psi}{\partial \mathbf{e}}, \quad \mathbf{r} = \frac{\partial \psi}{\partial \mathbf{u}}, \quad \mathbf{K} = \frac{\partial^2 \psi}{\partial \mathbf{u} \partial \mathbf{u}}. \tag{7}$$

Constitutive equations (3) of the members of tensegrity assemblies differ for struts and cables. In order to treat the unilateral behavior of cables and the deep postbuckling behavior of struts the concept of the "equivalent bar" is introduced. According to this concept all members remain straight at every stage of deformation. Constitutive equations of such an equivalent system may be obtained by observing behavior of real cables and struts in terms of $\mathbf{p}$ and $\mathbf{e}$. Column matrix $\mathbf{e}$ includes the chord length elongations, the elongations of straight lines connecting corresponding nodes. Generally, these elongations are not equal to the difference between final and initial length of the members. Column matrix $\mathbf{p}$ includes the appropriate member forces acting at the nodes and directed along straight lines connecting corresponding nodes. Entries of $\mathbf{p}$ are not necessarily tangent to the longitudinal axes of corresponding members. These cautions regarding the physical and geometrical meaning of $\mathbf{p}$ and $\mathbf{e}$ are important when the postbuckling of struts and compression of cables are considered.

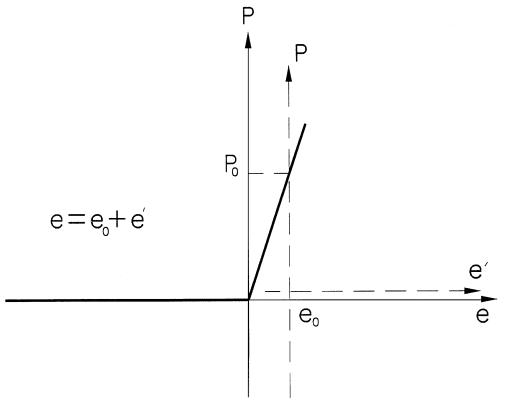

Fig. 3. Constitutive relations for unilateral microfilaments: chord elongation versus axial force. The horizontal shift is used to define initial pre-stressing.

The constitutive law for a cable member, or its equivalent bar, is shown graphically in Fig. 3. The cable does not resist compression and resists tension linearly, according to Hooke's law. The bold line indicates initially unstressed state of an ideal cable. In practical cases the cable is initially tensioned by p_0 and by using the shifting of coordinates shown by dotted lines it is possible to obtain the corresponding constitutive relations. The shifting is horizontal with e_0 corresponding to p_0. Vertical shifting is not necessary when the pretensioned configuration is considered as the initial one. Constitutive equations take the form

$$p=\begin{cases}0, & -\infty<e\leqslant -e_0 \quad (-\infty<p\leqslant 0)\\ S(e+e_0), & -e_0<e<+\infty \quad (0<p<+\infty),\end{cases} \tag{8}$$

$$\psi=\begin{cases}0, & -\infty<e\leqslant -e_0 \quad (-\infty<p\leqslant 0)\\ S(e+e_0)^2/2, & -e_0<e<+\infty \quad (0<p<+\infty),\end{cases} \tag{9}$$

where $S=EA/L$ is the cable stiffness coefficient (E, Young modulus; A, cross-sectional area; L, member length). Since cable elements do not undergo large changes of the chord length in tension (and they are switched off in compression) it is possible to define kinematic relations of an individual member as follows:

$$e=l-L=\varepsilon+\omega, \tag{10}$$

$$\varepsilon=(X_j-X_s)\frac{u_j-u_s}{L}+(X_{j+1}-X_{s+1})\frac{u_{j+1}-u_{s+1}}{L}+(X_{j+2}-X_{s+2})\frac{u_{j+2}-u_{s+2}}{L}, \tag{11}$$

$$\omega=\frac{1}{2L}\{(u_j-u_s)^2+(u_{j+1}-u_{s+1})^2+(u_{j+2}-u_{s+2})^2\}, \tag{12}$$

where L and l are the initial and final chord lengths of the member, respectively; u and X are nodal displacements and coordinates, respectively.

The constitutive law for a strut member, or its equivalent bar, is shown graphically in Fig. 4. The bold line indicates initially unstressed state of an ideal strut. The strut resists tension and compression linearly in accordance with Hooke's law up to the critical force p_{cr}. When the critical point is passed, the post-buckling behavior begins as shown schematically in the figure. Again, considering the initial stress and shifting coordinates it is possible to write constitutive equations as follows:

$$p=\begin{cases}f[e+e_0], & -\infty<e\leqslant e_{cr}-e_0 \quad (-\infty<p\leqslant p_{cr})\\ S(e+e_0), & e_{cr}-e_0<e<+\infty \quad (p_{cr}<p<+\infty),\end{cases} \tag{13}$$

$$\psi=\begin{cases}\int f[e+e_0]\mathrm{d}e, & -\infty<e\leqslant e_{cr}-e_0 \quad (-\infty<p\leqslant p_{cr})\\ S(e+e_0)^2/2, & e_{cr}-e_0<e<+\infty \quad (p_{cr}<p<+\infty),\end{cases} \tag{14}$$

where $S=EA/L$ is the strut stiffness coefficient (E, Young modulus; A, cross-sectional area; L, member length). Eqs. (13) and (14) contain function $f[e]$ which can not be written explicitly. This function is obtained from the solution of the 'elastica' problem (Timoshenko and Gere, 1961)

$$\frac{p}{p_{cr}}=\frac{4}{\pi^2}K\left[\sin\frac{\alpha}{2}\right]^2, \tag{15}$$

$$l[\alpha]=L\left(\frac{4}{\pi}\sqrt{\frac{p_{cr}}{p}}E\left[\sin\frac{\alpha}{2}\right]-1\right), \tag{16}$$

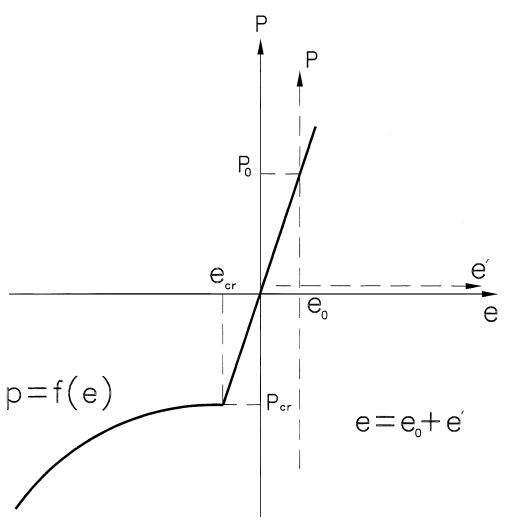

Fig. 4. Constitutive relations for buckling microtubules: chord elongation versus axial force. The horizontal shift is used to define initial pre-stressing.

where l is the strut chord length after the deformation; $K[\bullet]$ and $E[\bullet]$ are complete elliptic integrals of the first and second kind correspondingly; $p_{cr} = \pi^2 EI/L^2$ is the usual critical load; and α is the edge slope. To find a polynomial spline expressing $p \sim e$ relations analytically one should tabulate relation $p \sim \alpha$ from Eq. (15), then substitute corresponding values of p and α into Eq. (16) and tabulate the desirable $p \sim e$ relations. It is physically clear that this relation should be smooth and monotone and, thus, even low-order polynomials are expected to provide a good accuracy. Finally, Eqs. (13) and (14) take the form

$$p = \begin{cases} \beta_0 + \beta_1(e+e_0) + \beta_2(e+e_0)^2 + ,\ldots, & -\infty < e \leqslant e_{cr} - e_0 \quad (-\infty < p \leqslant p_{cr}) \\ S(e+e_0), & e_{cr} - e_0 < e < +\infty \quad (p_{cr} < p < +\infty) \end{cases} \tag{17}$$

$$\psi = \begin{cases} \beta_0(e+e_0) + \beta_1(e+e_0)^2/2 + \ldots, & -\infty < e \leqslant e_{cr} - e_0 \quad (-\infty < p \leqslant p_{cr}) \\ S(e+e_0)^2/2, & e_{cr} - e_0 < e < +\infty \quad (p_{cr} < p < +\infty) \end{cases} \tag{18}$$

The polynomial coefficients β_i are obtained by using the least-squares approximation as described previously. The chord elongation of an arbitrary strut takes the following form:

$$e = l - L, \tag{19}$$

$$l = \sqrt{(X_j + u_j - X_s - u_s)^2 + (X_{j+1} + u_{j+1} - X_{s+1} - u_{s+1})^2 + (X_{j+2} + u_{j+2} - X_{s+2} - u_{s+2})^2}, \tag{20}$$

$$L = \sqrt{(X_j - X_s)^2 + (X_{j+1} - X_{s+1})^2 + (X_{j+2} - X_{s+2})^2}. \tag{21}$$

These kinematic relations cannot be simplified as it was done for cables because the change in the chord length may be significant at the postbuckling stage.

Numerical simulation is carried by using Mathematica software (Wolfram, 1991) allowing both symbolic and numeric computations. In this case the tangent stiffness matrix **K** and the internal nodal force **r** are obtained symbolically according to Eq. (7). In order to avoid multiple calculations of **K** and **r** corresponding to pre- and post-buckling for struts and compression and tension for cables the following strategy was used. Both contributions (14_1) and (14_2) are included into the general strain energy expression for cables as well as contributions (18_1) and (18_2) for struts. These terms are multiplied by "switching functions", which take only two values 0 or 1 according to the magnitude of the forces of the corresponding members. For example, if the strut member force is greater than p_{cr} then the "switching functions" of (18_1) takes zero value while "switching functions" of (18_2) takes unity value. The cable elements are "switched" in the same manner. Computations are performed by using incremental loading and Newton–Raphson technique is applied at every increment. The "switching functions" are compared at the beginning and at the end of every increment. If they remain unchanged, then the subsequent load increment is applied, if not, the analysis is performed again by switching the corresponding function beforehand. This repetition of the analysis is necessary for the compressed struts since their behavior changes drastically. This is not the case of cables and thus the switch was done on subsequent increment when necessary.

Two examples of tensegrity cells shown in Figs. 2 and 1 are considered. The first one is a plane structure composed of four struts connected by eight cables; the second one is a space structure composed of six struts connected by 24 cables. Both structures are supported as shown in the figures in order to exclude rigid body motions. Simple geometry considerations give the following relations between the reference chord lengths of the struts and the cables for the plane and the space structures, respectively

$$L_C = L_S\sqrt{2-\sqrt{2}}/2, \tag{22}$$

$$L_C = L_S\sqrt{3/2}/2. \tag{23}$$

Nodal equilibrium at the reference state gives the following relations between the strut compression forces and the cable tension forces for the plane and the space structures, respectively

$$p_S = 2p_C\cos(3\pi/8), \tag{24}$$

$$p_S = p_C\sqrt{6}. \tag{25}$$

In order to define and control the reference state the following procedure is used. The experimentally obtained length of microtubules 3 μm (Amos and Amos, 1991) is used for all strut members at rest (not at the reference state!). Bending stiffness $(EI)_S = 2.15\times10^{-23}\,\mathrm{Nm}^2$ (Couphlin and Stamenovich, 1997; Felgner et al., 1996) is used. Elasticity modulus and cross-sectional area are defined as follows (Gittes et al., 1993): $E_S = 1.2\,\mathrm{GPa}$, $A_S = 190\,\mathrm{nm}^2$. The constitutive diagram shown in Fig. 4 is obtained by using the above data. The postbuckling behavior is approximated by polynomial with $p_{cr} =$

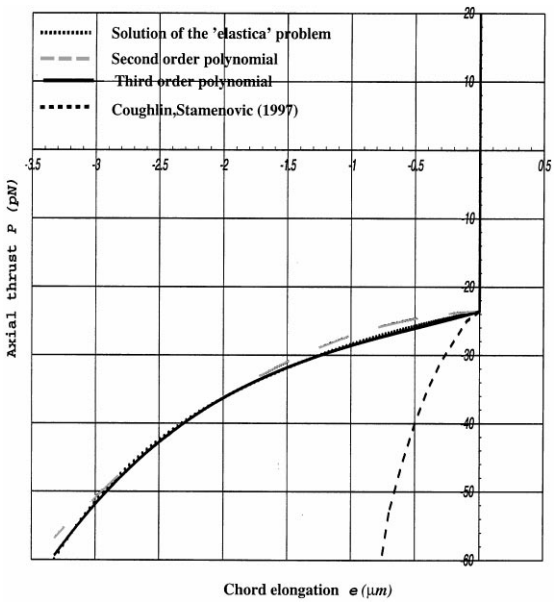

Fig. 5. Postbuckling of the microtubule of 3 μm length at rest: elastica (exact solution), second-order polynomial, third-order polynomial, asymptotic curve by Coughlin and Stamenovic (1997).

23.578 pN. Fig. 5 shows that both the second- and third-order polynomials give excellent accuracy. Also the results of Coughlin and Stamenovich (1997) are shown. It is evident that the latter results are acceptable at the critical point only and they diverge significantly from the correct curve in the whole postbuckling area. For arbitrary prestressing forces p_S of the struts, the corresponding reference chord lengths L_S are obtained from the constitutive diagram. By using Eqs. (22) and (24) for the plane structure or Eqs. (23) and (25) for the space structure it is possible to obtain the cable chord lengths L_C and forces p_C at the reference state. The approach described above is consistent since the cable length at rest is not defined beforehand. Filaments modeled by cables are assumed to be of appropriate length at rest and they possess the following elasticity modulus and cross sectional area (Gittes et al., 1993): $E_C = 2.6\,\text{GPa}$, $A_S = 18\,\text{nm}^2$; it is assumed that they have no bending stiffness and no ability to resist compression.

3. Results

The structural analysis of 2D and 3D models of living cells of tensegrity structure yields explanation to the linear stiffening behavior of the living cells observed in experiments. This behavior is crucially affected by the tensegrity architecture of the cytoskeleton considering the buckling of microtubules and switching off of microfilaments. Moreover, gradual buckling of individual microtubules is reflected in the transient softening response of the cell.

The 4-strut plane cell is self-equilibrated in its reference state where the cable-microfilament tension is 3 pN and corresponding strut-microtubule compression is obtained by using Eq. (24) (Fig. 6, top left). The cell is loaded by the torsion pair applied at the edges of strut number 2, and by the stretching force applied at the right edge of strut number 1. At the load level of $T = 3\,\text{pN}$ cables are switched off (Fig. 6, top right). At the load level of $T = 21\,\text{pN}$ two struts buckle (Fig. 6, bottom left). At the load level of $T = 50\,\text{pN}$ the cell shape is changed drastically (Fig. 6, bottom right). The relatioship between the applied force T and stiffness, defined as the ratio of the applied force to the displacement in its direction at the node number 4, is approximately linear when two microfilaments are switched off and two microtubules buckled (Fig. 7). The latter happens when $T > 21\,\text{pN}$. Before this stage, however, the stiffness decreases, and softening is observed. This transient stage corresponds to the switching off of microfilaments and buckling of microtubules. After these abrupt changes the cell behavior becomes more stable and the linear stiffening is observed. Qualitatively similar results are obtained in numerical simulations of the 3D cell model. Vertical "shearing" forces applied at nodes 1,2,10,12 of the space cell (Fig. 8). The cell reference state corresponds to the microtubules' compression of 2.5 pN. The force/stiffness dependence at the node number 1, shown in Fig. 9, exhibits again transient softening behavior when cables are switched off and struts buckle, which is followed by stable linear stiffening.

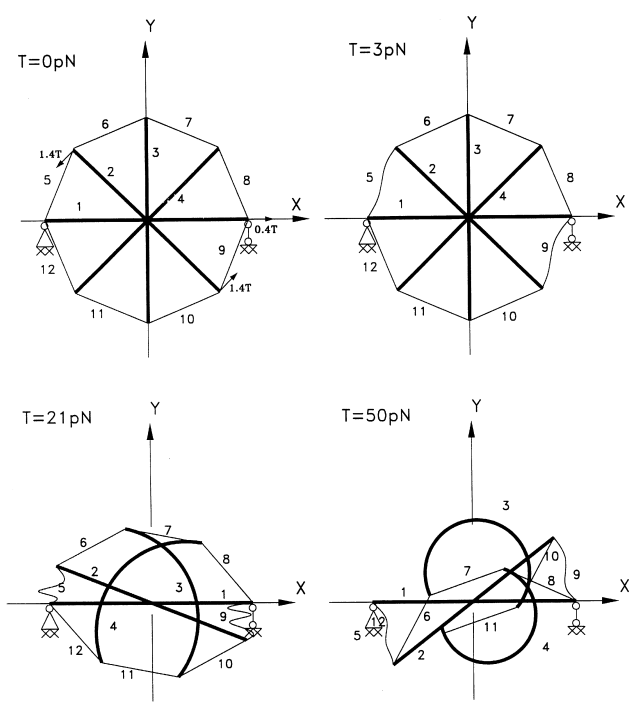

Fig. 6. Schematic loading history of the plane cell. Initially all members are straight (top left). The 5th and 9th microfilaments are switched off in the beginning of loading (top right). Then the 2nd and 4th microtubules buckle (bottom left). These stages define the overall cell softening. Finally the behavior of individual members is stabilized (bottom right) and the overall linear stiffening begins.

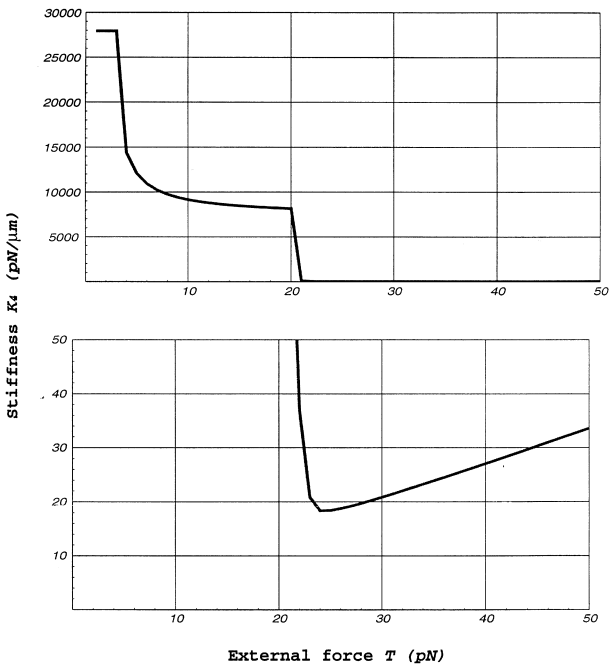

Fig. 7. Force versus stiffness at the 4th node of the plane cell. Softening takes place at loads below 24 pN. Linear stiffening takes place at loads larger than 24 pN in accordance with qualitative history shown in Fig. 6.

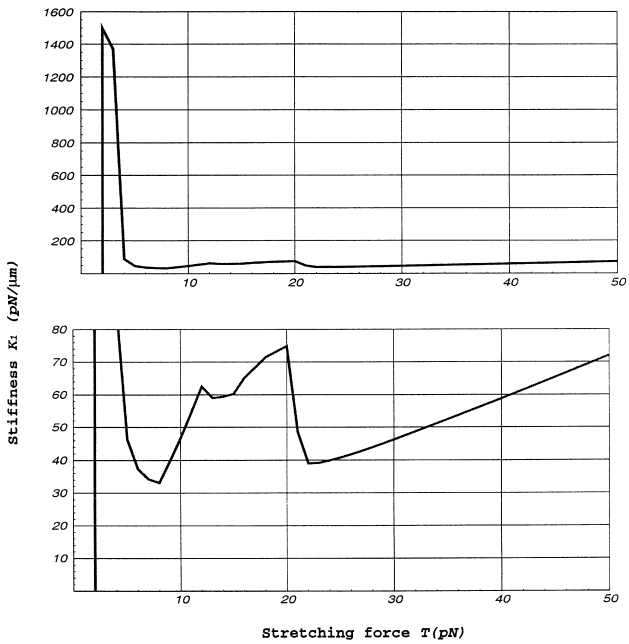

Fig. 9. Force versus stiffness at the 1st node of the space cell. Also in this case the stable linear stiffening at loads larger than 22 pN can be observed.

4. Discussion

A theoretical explanation to the linear stiffening of living cells was addressed by modeling the cytoskeleton as a tensegrity structure. For this purpose a novel computational framework allowing consideration of unilateral mechanical response of the cables-microfilaments and deep postbuckling behavior of the struts-micro-

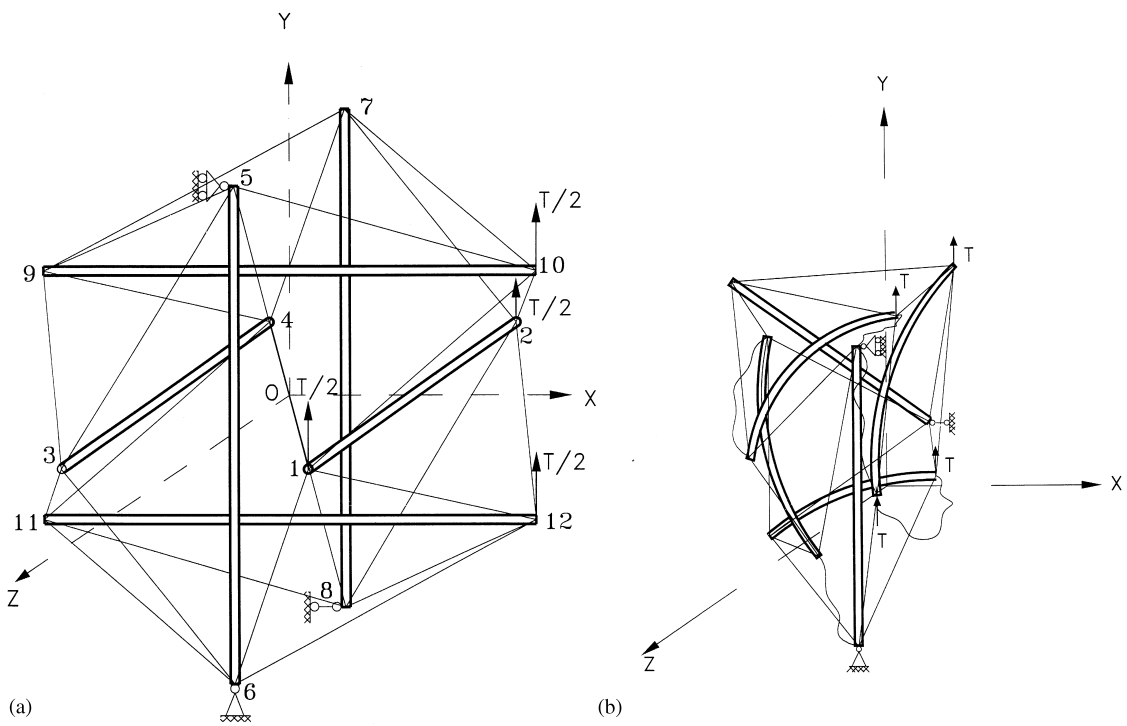

Fig. 8. (a) "Shearing" loading of the space cell model; (b) A schematic state of the cell when the linear stiffening begins.

tubules was developed. This framework allowes tracing the mechanical response of a cell considering deep postbuckling of extremely flexible microtubules. The latter is in contrast to the previous work of Coughlin and Stamenovich (1997) where the analysis of buckled microtubules was based on asymptotic techniques, that are appropriate for the qualitative prediction of the initial postbuckling stage only. However, these asymptotic techniques fail when the full-scale nonlinear analysis is necessary (Fig. 5).

The *linear stiffening* of the cytoskeleton models was obtained in computer simulations which is in a very good qualitative agreement with experimental observations of Wang et al. (1993) and Wang and Ingber (1994), Thoumine et al. (1995). The linear stiffening may be explained as a result of the dominance of the buckled struts on the overall cell behavior. In this case, linear stiffening of individual buckled struts is directly correlated to the high accuracy of the second-order polynomial approximation of their post-buckling behavior (Fig. 5). These numerical results reinforce Ingber's tensegrity assumption.

A *transient softening* of the tensegrity models was discovered. This behavior is related to the abrupt changes in the response of the individual members of tensegrity assemblies: switching off of unilateral filaments and buckling of slender microtubules. After the microtubules buckled and appropriate filaments are switched off a stable stiffening phase is achieved. The transient softening has not been directly observed in experiments yet. However, the indirect confirmation of the softening may be extracted from recent experiments of Heidemann et al. (1999). These authors discovered the local response of the cytoskeleton to the local loads. They concluded that "this local accommodation and dissipation of force is inconsistent with the proposal that cellular tensegrity determines cell shape". This conclusion may be correct in the case where the possible local buckling of microtubules is ignored, and thus the tensegrity cell responds globally even to the local load. Previous models of tensegrity were indeed of this type, but more accurate tensegrity models allowing for buckling of flexible microtubules admit the local response to the local loads. In this view, the cited experiments may be interpreted in favor of the tensegrity assumption and explained by the local buckling of the microtubules and switching off of the filaments.

Presented analysis and its conclusions are restricted by two 2D and 3D relatively simple examples of tensegrity cells comprising 12 and 30 elements, respectively. Evidently, in real cells the number of elements is significantly larger. However, there is a clear similarity in the behavior of two different examined models: both of them exhibit transient softening and linear stiffening. This fact supports belief that increasing number of the model elements cannot crucially change qualitative results. The load level where stiffening or softening occurs surely depends on the behavior of individual microtubules and microfilaments, the overall response, however comprise only two qualitative stages mentioned above.

Numerical simulations of mechanical loading of space and plane tensegrity models of the cell cytoskeleton explain theoretically ("from first principles") the linear stiffening behavior of living cells observed in experiments. Such a coincidence supports Ingber's assumption of the crucial role of the cytoskeleton tensegrity architecture in mechanical behavior of cells. These numerical simulations also predict a new kind of the overall cell behavior: softening. The softening was not observed in experiments directly. However, some recent experimental results (Heidemann et al., 1999) may be readily explained within the frame of the softening behavior. The latter is again in favor of the tensegrity architecture of the cytoskeleton.

References

Amos, L.A., Amos, W.B., 1991. Molecules of the Cytosceleton. Guilford Press, New York.

Coughlin, M.F., Stamenovich, D., 1997. A tensegrity structure with buckling compression elements: application to cell mechanics. ASME Journal of Applied Mechanics 64, 480–486.

Felgner, H., Frank, R., Schilwa, M., 1996. Flexural rigidity of microtubules measured with the use of optical tweezers. Journal of Cell Science 109, 509–516.

Gittes, F., Mickey, B., Nettleton, J., Howard, J., 1993. Flexural rigidity of microtubules and actin filaments measured from thermal fluctuations in shape. Journal of Cell Biology 120, 923–934.

Harris, A.K., Wild, P., Stopak, D., 1980. Silcone rubber substrata: a new wrinkle in the study of cell locomotion. Science 208, 177–180.

Heidemann, S.R, Kaech, S., Buxbaum, R.E., Matus, A., 1999. Direct observations of the mechanical behavior of the cytoskeleton in living fibroblasts. Journal of Cell Biology 145, 109–122.

Ingber, D.E., 1993. Cellular tensegrity: defining new rules of biological design that govern the cytosceleton. Journal of Cell Science 104, 613–627.

Ingber, D.E., 1998. The architecture of life. Scientific American, January.

Maniotis, A.J., Chen, C.S., Ingber, D.E., 1997. Demonstration of mechanical connections between integrins, cytoskeletal filaments, and nucleoplasm that stabilize nuclear structure. Proceedings of the National Academy of Sciences USA 94, 849–854.

Thoumine, O., Ziegler, T., Girard, P.R., Nerem, R.M., 1995. Elongation of confluent endothelial cells in culture: the importance of fields of force in the associated alterations of their cytosceletal structure. Experimental Cell Research 219, 427–441.

Timoshenko, S.P., Gere, J.M., 1961. Theory of Elastic Stability, 2nd Edition. McGraw-Hill, New York.

Volokh, K.Yu., 1999. Non-linear analysis of underconstrained structures. International Journal of Solids & Structures 36, 2175–2187.

Volokh, K., Yu., Vilnay, O., 1997a. New classes of reticulated underconstrained structures. International Journal of Solids & Structures 34, 1093–1104.

Volokh, K., Yu., Vilnay, O., 1997b. "Natural", "kinematic" and "elastic" displacements of underconstrained structures. International Journal of Solids & Structures 34, 911–930.

Wang, N., Butler, J.P., Ingber, D.E., 1993. Mechanotransduction across the cell surface and through the cytosceleton. Science 260, 1124–1127.

Wang, N., Ingber, D.E., 1994. Control of cytosceletal mechanics by extracellular matrix, cell shape, and mechanical tension. Biophysical Journal 66, 2181–2189.

Wolfram, S., 1991. Mathematica: A System For Doing Mathematics By Computer, 2nd Edition. Addison-Wesley, New York.